Mind the trap Non-negligible effect of volatile trapping in ice on C/O ratios in protoplanetary disks and exoplanetary atmospheres

Ligterink, N. F.W.; Kipfer, K. A.; Gavino, S.

DOI
10.1051/0004-6361/202450405

Publication date
2024

Document Version
Final published version

Published in
Astronomy and Astrophysics

A&A, 687, A224 (2024)
https://doi.org/10.1051/0004-6361/202450405

Astronomy & Astrophysics

Mind the trap

Non-negligible effect of volatile trapping in ice on C/O ratios in protoplanetary disks and exoplanetary atmospheres

N. F. W. Ligterink[1,2], K. A. Kipfer[1], and S. Gavino[3]

[1] Space Research & Planetary Sciences, Physics Institute, University of Bern, Sidlerstrasse 5, 3012 Bern, Switzerland
e-mail: niels.ligterink@unibe.ch
[2] Faculty of Aerospace Engineering, Delft University of Technology, Delft, The Netherlands
e-mail: niels.ligterink@tudelft.nl
[3] Niels Bohr Institute, University of Copenhagen, Øster Voldgade 5–7, 1350, Copenhagen K, Denmark

Received 16 April 2024 / Accepted 10 June 2024

ABSTRACT

Aims. The ability of bulk ices (H_2O, CO_2) to trap volatiles has been well studied in any experimental sense, but largely ignored in protoplanetary disk and planet formation models as well as the interpretation of their observations. We demonstrate the influence of volatile trapping on C/O ratios in planet-forming environments.
Methods. We created a simple model of CO, CO_2, and H_2O snowlines in protoplanetary disks and calculated the C/O ratio at different radii and temperatures. We included a trapping factor, which partially inhibits the release of volatiles (CO, CO_2) at their snowline and releases them instead, together with the bulk ice species (H_2O, CO_2). Our aim has been to assess its influence of trapping solid-state and gas phase C/O ratios throughout planet-forming environments.
Results. Volatile trapping significantly affects C/O ratios in protoplanetary disks. Variations in the ratio are reduced and become more homogeneous throughout the disk when compared to models that do not include volatile trapping. Trapping reduces the proportion of volatiles in the gas and, as such, reduces the available carbon- and oxygen-bearing molecules for gaseous accretion to planetary atmospheres. Volatile trapping is expected to also affect the elemental hydrogen and nitrogen budgets.
Conclusions. Volatile trapping is an overlooked, but important effect to consider when assessing the C/O ratios in protoplanetary disks and exoplanet atmospheres. Due to volatile trapping, exoplanets with stellar C/O have the possibility to be formed within the CO and CO_2 snowline.

Key words. astrochemistry – molecular processes – planets and satellites: atmospheres – protoplanetary disks

1. Introduction

Water (H_2O), carbon dioxide (CO_2), and carbon monoxide (CO) are some of the most abundant molecules found in the interstellar medium and planet-forming environments, specifically on ice-coated dust grains (Boogert et al. 2015). Due to their prominence and widespread availability, the physicochemical processes involving these molecules have been extensively studied in the laboratory (e.g. Hama & Watanabe 2013; Van Dishoeck et al. 2013; Linnartz et al. 2015). This includes their thermal desorption behaviour and the interplay of these molecules during desorption. Their desorption temperatures differ significantly, with the monolayer coverage peak desorption temperatures measured in the laboratory, ranging from ~30–40 K for the hypervolatile CO, ~80–90 K for CO_2, and to around 155–175 K for H_2O (Minissale et al. 2022). In fact, out of all prominent ice mantle components (e.g. also including CH_4, NH_3, and CH_3OH), water is the least volatile. Combined with its high abundance, H_2O ice serves as an important surface onto which molecules can adsorb and react, but also as a medium into which volatile species can be trapped (Bar-Nun et al. 1985; Collings et al. 2004). This way of locking up atoms and molecules is sometimes listed as mechanical trapping, entrapment, or physical trapping, but it is always related to the ability of a bulk medium to cover up a single or cluster of species and preserve them in the ice matrix. Laboratory experiments have shown that large fractions of volatile molecules can be trapped well above their peak desorption temperature. An example is given in Fig. 1, which shows a temperature programmed desorption (TPD) trace of a mixed H_2O:CO_2:CO ice adapted from Kipfer et al. (2024a). As the ice is linearly heated, the release of these molecules is followed with a mass spectrometer. The molecules sublimate at their characteristic pure temperatures (1, 2, 4), but CO and CO_2 also release well above their desorption temperature. Carbon monoxide co-releases with CO_2 (2), while CO and CO_2 both also release with the water sublimation event. This happens in the form of co-desorption with H_2O at ~170 K (4) and in the form of a volcano desorption event at ~145 K (3), which occurs when water-ice rearranges from an amorphous to crystalline structure and volatile species are expulsed from the ice (Burke & Brown 2010). Water ice can trap fractions of over tens of percent and up to a hundred percent of added volatiles, depending on the molecule or atom involved, ice structure, ice formation temperature, mixing ratios, and deposition rate (Bar-Nun et al. 1985; Notesco et al. 2003; Collings et al. 2004; Fayolle et al. 2011; Almayrac et al. 2022; Simon et al. 2023; Kipfer et al. 2024a). Similar trapping efficiencies have been found for CO_2 ice as bulk medium (Simon et al. 2019). A more detailed description of how desorption and trapping fractions are determined in laboratory experiments is provided in Appendix A. The trapping

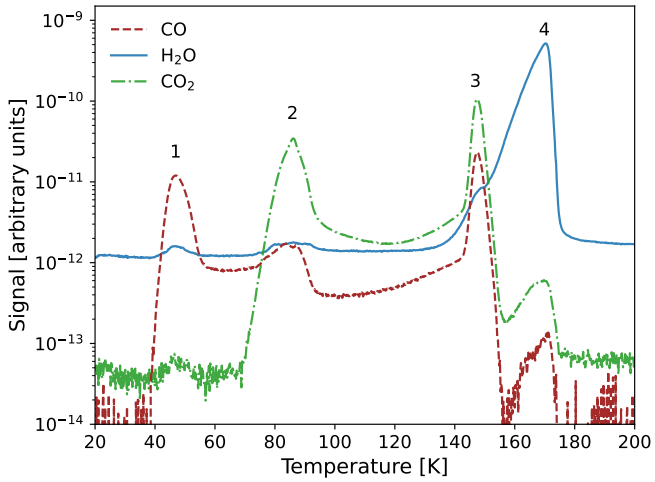

Fig. 1. Thermal desorption of a mixed H_2O:CO_2:CO ice film at 100:15:5 ratio recorded during a Temperature Programmed Desorption (TPD) experiment, where the release of each molecule is measured with a mass spectrometer. Carbon monoxide was traced with the ^{13}CO isotope. Four distinct release events are visible: pure-phase CO (1), pure-phase CO_2 with CO co-desorbing (2), volcano desorption of CO and CO_2 (3), and water desorption with co-desorption of CO and CO_2 (4). Desorption and trapping fractions of volatiles can be determined by integrating the TPD trace over discrete temperature ranges. The data are adapted from Kipfer et al. (2024a).

of volatiles affects the physical and chemical processes in star and planet-forming environments, but nuanced differences are expected between trapping in a laboratory and natural environment. For example, Ciesla et al. (2018) showed that efficient trapping takes place when the timescale for a volatile species to desorb is longer than the time it takes to be covered by a monolayer of water; this is the so-called 'burial regime'. These conditions are met at high deposition rates, as usually used in laboratory experiments, or when surface temperatures are low. Considering the low temperatures at which H_2O formation takes place on interstellar dust grains (Hama & Watanabe 2013), it is expected that experimentally determined trapping efficiencies apply to interstellar environments. However, slow deposition in interstellar environments and at elevated temperatures will likely result in different trapping efficiencies.

Planets are thought to form in protoplanetary disks by the accretion of gas and ice-coated dust grains, pebbles, or planetesimals (e.g. Johansen et al. 2007; Lambrechts & Johansen 2012; Bitsch et al. 2019; Lambrechts et al. 2019). The bulk molecular species contained in solids and in gas play a prominent role in setting the elemental composition of a planet. Öberg et al. (2011b) presents a model of the radially varying gas phase and solid-state carbon-over-oxygen (C/O) ratio in a protoplanetary disk, due the step-wise release of CO, CO_2, and H_2O from the ice to the gas. The model predicts that the C/O ratio of a planetary atmosphere depends on which side of the major volatile ($CO/CO_2/H_2O$) snowlines the object is formed. A high C/O ratio (>0.8) indicates that the formation was initiated outside the snowlines prior to inward migration (Madhusudhan et al. 2014). An exoplanet transit is typically used to derive the atmospheric composition and a significant number of C/O ratio values have now been measured (Hoch et al. 2023). The Öberg et al. (2011b) model has been used to determine the formation location of exoplanets based on their observed atmospheric C/O ratio (Mollière et al. 2020; Zhang et al. 2021). For instance, the supersolar gas phase C/O ratio ($\gtrapprox$0.55) outside the water snowline was used to explain the C/O ≥1 ratio measured in the atmosphere of the exoplanet WASP-12b (Madhusudhan et al. 2011). Conversely, the low C/O ratio measured in the atmosphere of WASP-77Ab is interpreted as a formation scenario where the atmospheric material is accreted inside the major snowlines (Line et al. 2021). In the last decade, more refined models to predict protoplanetary disk snowlines and C/O ratios have been presented in the literature, which includes solid-state and gas phase chemical processes, grain growth, or novel physical processes (Owen 2020; Notsu et al. 2020; Cridland et al. 2020; Zhang et al. 2020a; Eistrup et al. 2022; Gavino et al. 2023). However, the trapping of volatiles within the matrix of bulk H_2O and/or CO_2 has largely been ignored in the models (Schneeberger et al. 2023), despite that formalisms for volatile trapping have been included in a select number of astrochemical models (Viti et al. 2004; Visser et al. 2009; Taquet et al. 2012; Garrod et al. 2022).

In this paper, we revisit the static model of Öberg et al. (2011b) and include volatile trapping to show that this has a non-negligible effect on the C/O ratio in a protoplanetary disk and (exo)planets that form there. In Sect. 2, we describe the modified model and show how trapping affects solid-state and gas phase C/O ratios in protoplanetary disks. In Sect. 3, these results and their implications for protoplanetary disk and exoplanet atmosphere C/O ratios are discussed.

Table 1. Model parameters.

Molecule	T (K)	n_O $10^{-4} \times n_H$	n_C $10^{-4} \times n_H$
CO	20	1.5	1.5
CO_2	47	0.6	0.3
H_2O	135	0.9	–
Carbon grains	500	–	0.6
Silicate	1500	1.4	–

Notes. Model parameters are adopted from Öberg et al. (2011b), which in turn are based on data from Pontoppidan (2006), Draine (2003), and Whittet (2010).

2. Model and results

To determine the protoplanetary disk C/O ratio, we adopted the static snowline model presented in Öberg et al. (2011b). In short, this model assumes that CO, CO_2, and H_2O ices fully sublimate at distinct sublimation temperatures, that is, their respective snowlines. At each snowline, one molecular species desorbs, which results in the depletion of solid carbon and/or oxygen, while simultaneously setting or modifying the gas phase elemental budget. Carbon grains and silicates are significant elemental carriers, but sublimate at much higher temperatures than H_2O. Therefore, they remain solid in the temperature range used in this model and only affect the solid carbon and oxygen budget. The model parameters, namely, the sublimation temperatures and elemental abundances per molecule, are presented in Table 1. The relative abundances between H_2O, CO_2, and CO are (in that order) 0.9:0.3:1.5 and are derived from the CBRR 2422.8-3423 protoplanetary disk (Pontoppidan 2006). We note that sublimation temperatures differ from the aforementioned laboratory desorption temperatures, due to the difference in heating timescale. Snowlines are plotted on a protoplanetary disk temperature profile following the equation $T = T_0 r^{-q}$, where T_0 = 200 K, r is the radius in a.u., and q is the power law index of 0.62

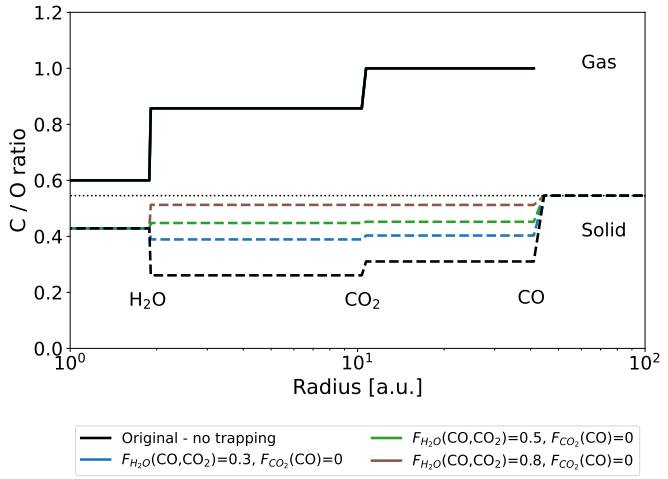

Fig. 2. Gas phase and solid-state C/O ratios at various radii in a protoplanetary disk, based on the trapping and release of CO, CO_2, and H_2O. The original model of Öberg et al. (2011b) without trapping is presented in black. The updated model takes the trapping of CO and CO_2 in H_2O (F_{H_2O}(CO,CO_2)) and CO in CO_2 (F_{CO_2}(CO)) at different fractions into account (blue, green, and red lines) and shows that the solid C/O ratio is strongly affected. The snowlines of CO, CO_2, and H_2O are indicated.

(Andrews & Williams 2007), where smaller radii correspond to higher temperatures and larger radii to lower temperatures. The resulting radial gas phase and solid-state C/O distributions of the original Öberg et al. (2011b) model (black line) are shown in Fig. 2. This model does not take volatile trapping into account.

We modified the above model to include volatile trapping by releasing a fraction of the volatiles with water (F_{H_2O}(CO,CO_2)) or CO_2 (F_{CO_2}(CO)). Volatile release associated with water sublimation occurs in two ways: volcano desorption, namely, the rapid release of volatiles during the amorphous to crystalline phase change of ice, and co-desorption, namely, the release of volatiles together water desorption (Burke & Brown 2010). Volcano desorption occurs at a lower temperature than the peak water sublimation temperature by approximately ~20% (Collings et al. 2004; Kipfer et al. 2024a). Experimental studies show that significant volatile release starts with (or is even dominated by) volcano desorption and continues until all volatiles are depleted during the water co-desorption event (Martín-Doménech et al. 2014). In the modified static model we release all volatiles interior of the water snowline, but we note that under realistic conditions loss of some CO and CO_2 will also occur leading up to the water snowline. Co-desorption of volatiles with CO_2 occurs at the CO_2 sublimation temperature (Simon et al. 2019; Kipfer et al. 2024a) and this is adopted as such in the modified model.

Over recent decades, many studies have determined which fractions of volatiles are trapped by H_2O and CO_2 (e.g. Bar-Nun et al. 1985; Collings et al. 2004; Fayolle et al. 2011; Ligterink et al. 2018; Simon et al. 2023; Kipfer et al. 2024a). Figure 3 shows a compilation of the literature results and presents trapping fractions plotted against the matrix: volatile mixing ratio and the ice layer thickness given in monolayers (ML, 1 ML = 10^{15} molecules cm^{-2}). The data and methods to determine trapping fractions are described in Appendix A. In general, thicker ice films trap more volatiles, while a large volatile concentration results in a smaller fraction of volatiles being trapped. From this overview, we can say that trapping fractions in an ice mantle are F_{CO_2}(CO) = 0.1–0.7, F_{H_2O}(CO_2) = 0.3–0.95, and

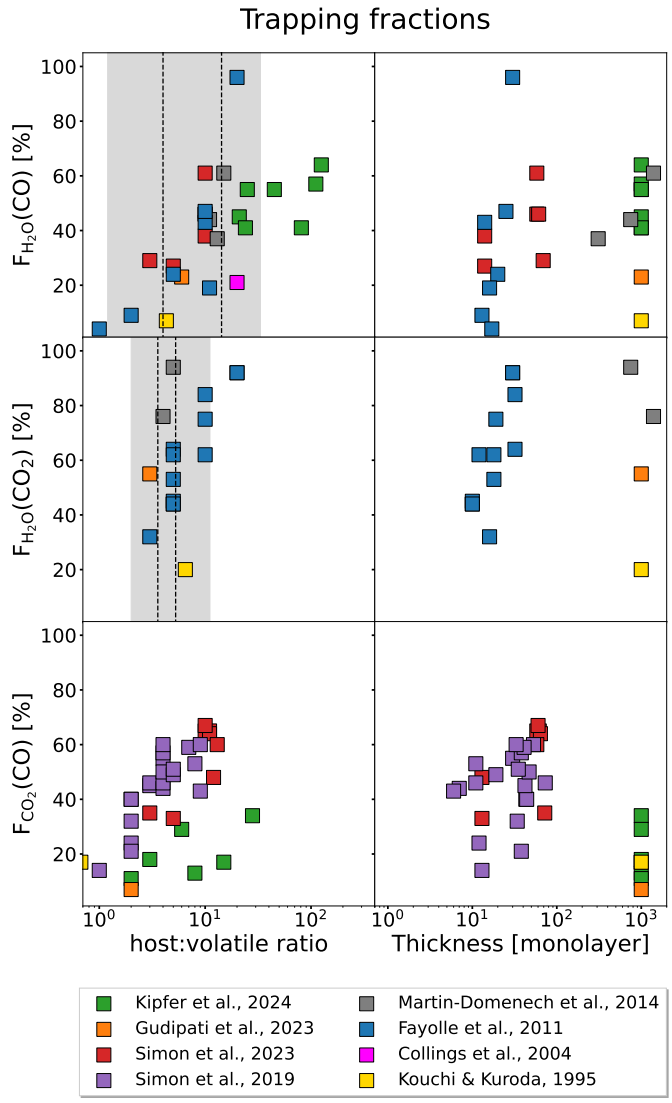

Fig. 3. Trapping efficiencies of CO and CO_2 in water (F_{H_2O}(CO,CO_2)), and CO in CO_2 (F_{CO_2}(CO)) plotted against the host: volatile ice ratio (left) and the ice layer thickness (right). The thickness is given in monolayer (ML), where 1 ML = 10^{15} molecules cm^{-2}. The grey shaded boxes show the H_2O:CO and H_2O:CO_2 ice ratios observed in a variety of interstellar sources, while the dashed lines show their largest and smallest median values for data presented in Boogert et al. (2015). The laboratory data used in this plot are presented in Table A.1.

F_{H_2O}(CO) = 0.2–0.7 for mixing ratios ≥5:1. We test the effect of various realistic trapping fractions in a series of model runs.

Figure 2 shows three models with water trapping fractions of F_{H_2O}(CO,CO_2) = 0.3, 0.5, and 0.8. Both CO and CO_2 are trapped in the same fraction. Trapping by CO_2 is ignored. We find that trapping has a significant effect on the solid-state C/O ratio, while it does not affect its gas phase counterpart. As larger fractions of CO and CO_2 are trapped in water ice, the variations in solid-state C/O ratio are reduced and can even be considered constant from outside the CO snowline up to the H_2O snowline for the largest fraction of trapping.

Figure 4 shows three models where CO and CO_2 are trapped in different fractions in water, at F_{H_2O}(CO,CO_2) = (0.3;0.5), (0.5;0.8), and (0.3;0.8). In the solid-state, this again results in a reduction in C/O variations. However, this time also the gas phase C/O ratio is affected, which becomes more homogeneous.

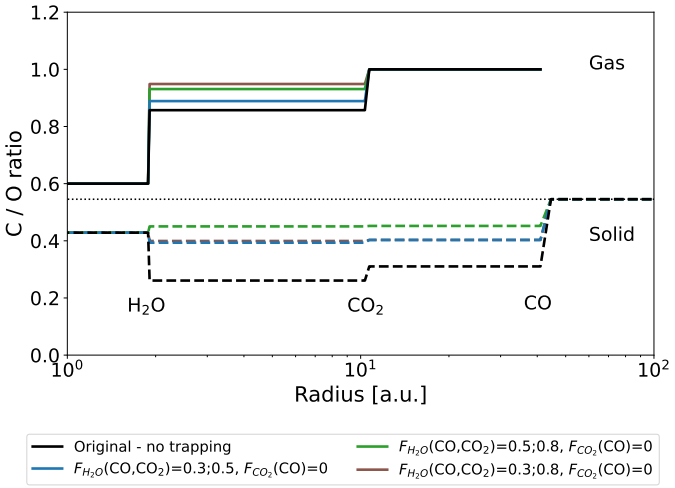

Fig. 4. Same as Fig. 2, but different trapping ratios of CO and CO_2 in H_2O.

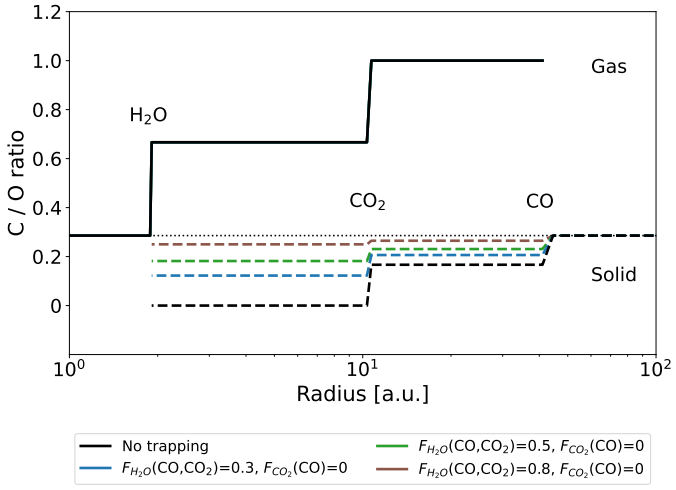

Fig. 5. Same as Fig. 2, but only for H_2O, CO_2, and CO at 100:25:25 ratio. The contributions of silicates to atomic oxygen and carbonaceous dust to atomic carbon are omitted.

Trapping of CO in CO_2 is included in Figs. B.1 and B.2. In general, reduction of variations and homogenisation of the solid-state and gas phase C/O ratios is seen again. The release of a fraction of CO with CO_2 causes a more pronounced drop in solid-state C/O ratio around the CO_2 snowline. We conclude that volatile trapping has a non-negligible effect on both solid-state and gas phase C/O ratios.

3. Discussion and implications

In the following sections, we discuss the results and implications from the perspective of interstellar ice compositions and laboratory data on trapping efficiencies, protoplanetary disks, and exoplanet atmospheres.

3.1. Ice composition and trapping efficiency

The modified model demonstrates that the trapping of volatiles affects the C/O ratio by reducing variations to this ratio. The extent of this reduction with respect to the solid material depends on the fraction of volatile that is trapped, while for the gas phase, it depends on the size of the difference between trapped fractions of volatiles. Laboratory experiments show that volatile trapping is efficient (see Fig. 3), but this efficiency decreases as the volatile concentration increases. For example, Fayolle et al. (2011) measured a CO trapping fraction in water of $F_{H_2O}(CO)$ = 0.04 for a 1:1 H_2O:CO ice film of 17 ML. Since the ice composition used in Öberg et al. (2011b) is 0.9:0.3:1.5 H_2O:CO_2:CO, that is, CO is ∼1.7 times more abundant than H_2O, this led to the claim that volatile trapping is negligible. While this might be the case for this particular ice composition, this mixing ratio is not representative of the ice generally found in the interstellar medium or protoplanetary disks (Boogert et al. 2015). For example, the median ice compositions presented in Öberg et al. (2011a) range from 100:38:31 H_2O:CO_2:CO for cloud cores to 100:13:13 for high-mass protostars. Similar patterns are seen for protoplanetary disks (Aikawa et al. 2012; Sturm et al. 2023), where H_2O is the dominant ice component. Figure 5, shows the model results for a realistic ice composition of H_2O:CO_2:CO at a 100:25:25 ratio, both with and without trapping. The contributions of oxygen from silicates and carbon from carbonaceous dust are omitted in this model. For mixing ratios of 4:1 H_2O to CO_2 or CO, $F_{H_2O}(CO_2)$ ≥40% and $F_{H_2O}(CO)$ ≥25% have been reported (Fayolle et al. 2011; Simon et al. 2023). As can be seen in Fig. 5, a trapping efficiency of 30% significantly affects the C/O ratio and causes the same kind of homogenisation as observed in the fiducial model.

Trapping of volatiles depends on the structure of the ice. For example, when volatile species are covered by a layer of water instead of mixed, the volatile can be fully trapped (May et al. 2013a,b, where trapping is defined as the release of volatiles during volcano and co-desorption with water sublimation). Astrochemical models have demonstrated that volatiles can be concentrated in the bottom layers of the ice mantle and subsequently be covered by H_2O as an ice mantle grows Garrod et al. (2022). Furthermore, a recent experimental work by Potapov et al. (2023) has shown that the UV irradiation of carbonaceous dust covered by H_2O ice results in significant formation of CO_2 at the dust-ice interface. Thus, covering of volatiles on ice-coated dust grains is plausible in planet-forming regions and results in trapping fractions that are substantially larger than those of mixed ice.

Most experimental trapping studies make use of binary ice mixtures and show that volatile trapping is efficient. However, this efficiency (that is, that of the trapped fraction) can decrease as more volatiles are included in the ice. For example, Kipfer et al. (2024a) shows that the fraction of N_2 trapped in water-ice is influenced by the amount of CO_2 that is included in N_2:CO_2:H_2O mixtures and decreases as more CO_2 is incorporated. This observation has been linked to competition for binding sites when multiple volatile species are present in a water-ice matrix (e.g. Simon et al. 2023; Ligterink et al. 2024). Ice mantles of grains in planet-forming environments often consist of more than five dominant components and understanding the trapping behaviour of such multicomponent mixtures is relevant to assessing how trapping affects C/O ratios. However, the number of studies that have been conducted on ice systems that approach the complexity of interstellar ice mantles is limited. For example, analysis of TPD data of H_2O:CO:CO_2:CH_3OH:NH_3 mixed ice systems presented in Martín-Doménech et al. (2014) suggests that trapping fractions of CO and CO_2 are similar to those of binary and ternary systems (see Fig. 3 and Appendix A). However, dedicated investigations of multi-component ice films are needed to

determine if this observation holds and how trapping efficiencies are affected by various ice components and compositions.

In this study, we focus on the elemental carbon and oxygen budget derived from H_2O, CO_2, and CO. However, molecules such as methane (CH_4) should be considered as well. This volatile molecule can also be efficiently trapped in H_2O and CO_2 (Simon et al. 2023). Furthermore, elemental ratios involving atomic nitrogen and hydrogen are also of interest and carriers of these atoms have also been shown to show efficiently in terms of trapping (e.g. N_2, see Kipfer et al. 2024a).

3.2. Protoplanetary disk snowlines and missing volatiles

Volatile trapping potentially has two prominent observable effects on protoplanetary disks. First, it reduces the proportion of volatiles, such as CO, which are available in the gas phase in regions where the volatile should not be frozen out. Simultaneous measurements of HD (hydrogen deuteride) and CO in disks indicate that these objects are depleted in CO by a factor 5–100 (McClure et al. 2016; Zhang et al. 2020b). To account for this depletion, various effects have been proposed, such as pebble growth, physical sequestration, and chemical processes (e.g. Krijt et al. 2018; Eistrup et al. 2018). Models that combine these processes can predict a CO depletion factor close to 100 (Krijt et al. 2020). Volatile trapping in ice will contribute to such depletion with trapping fractions of up to 95% (see Fig. 3) for thin film ice. However, orders of magnitude depletion are unlikely for thin ice films and are likely to require thicker ice mantles as found on pebbles (Bosman et al. 2018).

Second, trapping tends to 'inject' volatiles at multiple locations in the disk into the gas phase, resulting in a step-wise increase of volatile abundances towards the protostar. For example, CO will enter the gas phase when its pure-phase ice sublimates, when CO_2 desorbs, and at the onset of H_2O sublimation. Observations of such step-wise increases might be challenging, due to limited spatial resolution, optically thick emission, excitation temperatures, and the usage of indirect chemical tracers (e.g. N_2H^+, van't Hoff et al. 2017). However, hints of it might be seen in some studies, such as observations performed by Zhang et al. (2020a), where an enhanced gas phase CO level and C/H ratio were found inside the CO snowline of the HD 163296 protoplanetary disk. These authors assigned this observation to pebble drift, but an alternative explanation relates to the release of carbon-bearing volatiles during the water ice volcano desorption event (see Fig. 1). This increases the gaseous carbon budget, while gas phase oxygen and hydrogen levels remain comparatively low because H_2O does not yet sublimate.

Other mechanisms can contribute to a step-wise increasing emission or double emission line pattern in a disk. The presence of pure multiple snowlines of one volatile species can be due to the presence of multiple dust surface temperatures. Using a two-sized model, Gavino et al. (2023) predicted two pure CO snowlines in a T Tauri disk, the first one at a few tens of au, the second at 100–150 au from the central star. This effect does not require radial drift and relies only on the presence of multiple dust temperatures. The presence of multiple dust sizes and temperatures can also contribute to create a snowline shape that is spread out radially and vertically (Gavino et al. 2021) rather than marking an abrupt step-wise emission. Radial drift can also affect volatile snowlines. Cleeves (2016), using a simple parameterised model, showed that the removal of large grains in the outer disk reshapes the thermal structure that can create multiple CO snowlines.

Trapped volatiles may be chemically processed into more complex molecules and thus removed from the ice. As ice-coated grains near a protostar, their temperatures and amounts of impinging radiation increase, which results in enhanced chemical reactions (Potapov et al. 2023). Under these conditions, CO embedded in H_2O-ice is efficiently converted into CO_2 (van Scheltinga et al. 2022). In turn, CO_2 thermally reacts with NH_3 to form carbamic acid (NH_2COOH, Khanna & Moore 1999; Noble et al. 2014; Marks et al. 2023). The formation of much more complex and refractory molecules is possible as well (e.g. Qasim et al. 2023; Kipfer et al. 2024b), which will desorb at much higher temperatures (~200–400 K) and much closer to protostar (Ligterink & Minissale 2023).

Finally, it is worth pointing out that recent edge-on observations of HH 48 NE protoplanetary disk with JWST revealed that CO ice features extend to large disk heights, where the temperature is likely to be high enough that pure, surface-bound, CO ice should have sublimated (Sturm et al. 2023). One interpretation of this observation is that CO is trapped in other bulk ice components. This notion is supported by the fact that the CO ice IR feature observed in the disk is broader than that of pure CO measured in the laboratory, which can be the result of interactions of CO with a H_2O-rich environment. Therefore, this observation highlights the importance of volatile trapping and the effects it may have on the disk chemistry.

3.3. C/O ratio in exoplanet atmospheres

Exoplanets are thought to inherit their elemental abundances from the gas and solids at the location where they form in the parent protoplanetary disk. As such, the measured relative abundance of their chemical content can be used as a diagnostic of their formation pathway. In particular, the Öberg et al. (2011b) model shows that the C/O ratio in hot Jupiters atmospheres is expected to be a signpost for their formation location relative to the main volatile snowlines in the disk. The planets that accrete their envelope inside the water snowline result in an oxygen-rich atmosphere (assuming a carbon-depleted disk) and a subsolar C/O ratio (e.g. Cridland et al. 2016; Mordasini et al. 2016), which favours in situ formation scenarios. The model also predicts that atmospheres with superstellar C/O ratios imply the accretion of gas between the H_2O and CO snowline (and subsequent inward migration after the gas is dissipated), substellar C/O ratios imply the accretion of solids between the H_2O and CO snowline, and a stellar C/O ratio suggests that the exoplanet formed outside the CO snowline (e.g. Madhusudhan et al. 2011, 2014, 2017; Mollière et al. 2020; Zhang et al. 2021; Line et al. 2021). However, when volatile trapping is included, we find that solid C/O ratios outside and inside the CO snowline are similar, see Fig. 2. Therefore, the observation of a stellar C/O ratio in an exoplanet atmosphere does not automatically imply that this object was formed outside the CO snowline. Instead, stellar C/O can likely be acquired due to the formation of the planet between the H_2O and CO snowline. Furthermore, this can affect the ice chemical composition during inward pebbles drift and the subsequent elemental composition of the planet formed. In this scenario, the grains migrate and carry the frozen CO or CO_2 on the surface to their respective snowline, increasing locally the gas phase abundances (e.g. Booth et al. 2017). Volatile trapping should reduce the chemical enhancement at snowline locations while the drifting pebble surfaces retain more CO and CO_2 ice than predicted. Superstellar C/O ratios can still be explained by the accretion of gases, although volatile trapping does reduce the amount of available gaseous material.

4. Conclusions

In this study, we demonstrate that volatile trapping in bulk ice strongly affects C/O ratios in protoplanetary disks. Strong variations in the C/O ratios seen in models without trapping have been reduced. Solid elemental ratios become constant from outside the CO snowline to inside the H_2O snowline. While gas phase C/O ratios are still enhanced, trapping reduces the amount of carbon- and oxygen-bearing molecules available in the gas. A similar effect is expected for volatile molecules that set the budget of other elements, such as nitrogen and sulfur. The homogenisation of the C/O ratios ensures that planets can acquire a stellar C/O ratio outside and inside the CO snowline. Observations of C/O ratios in exoplanet atmospheres are therefore difficult to link to a specific formation location in a protoplanetary disk.

Acknowledgements. The authors thank E.G. Bøgelund, S.F. Wampfler, J. Drążkowska, D. Semenov, H. Cuppen and M.N. Drozdovskaya for useful discussions, and A. Cridland for feedback on the manuscript. N.F.W.L. and K.A.K. acknowledge support from the Swiss National Science Foundation (SNSF) Ambizione grant 193453 and NCCR PlanetS. S.G. acknowledges support from the Independent Research Fund Denmark (grant no. 0135-00123B).

References

Aikawa, Y., Kamuro, D., Sakon, I., et al. 2012, A&A, 538, A57
Almayrac, M. G., Bekaert, D. V., Broadley, M. W., et al. 2022, Planet. Sci. J.l, 3, 252
Andrews, S. M., & Williams, J. P. 2007, ApJ, 659, 705
Bar-Nun, A., Herman, G., Laufer, D., & Rappaport, M. 1985, Icarus, 63, 317
Bitsch, B., Izidoro, A., Johansen, A., et al. 2019, A&A, 623, A88
Boogert, A. C. A., Gerakines, P. A., & Whittet, D. C. B. 2015, ARA&A, 53, 541
Booth, R. A., Clarke, C. J., Madhusudhan, N., & Ilee, J. D. 2017, MNRAS, 469, 3994
Bosman, A. D., Tielens, A. G., & van Dishoeck, E. F. 2018, A&A, 611, A80
Burke, D. J., & Brown, W. A. 2010, PCCP, 12, 5947
Ciesla, F. J., Krijt, S., Yokochi, R., & Sandford, S. 2018, ApJ, 867, 146
Cleeves, L. I. 2016, ApJ, 816, L21
Collings, M. P., Anderson, M. A., Chen, R., et al. 2004, MNRAS, 354, 1133
Cridland, A. J., Pudritz, R. E., & Alessi, M. 2016, MNRAS, 461, 3274
Cridland, A. J., Bosman, A. D., & van Dishoeck, E. F. 2020, A&A, 635, A68
Draine, B. T. 2003, ARA&A, 41, 241
Eistrup, C., Walsh, C., & van Dishoeck, E. F. 2018, A&A, 613, A14
Eistrup, C., Cleeves, L. I., & Krijt, S. 2022, A&A, 667, A121
Fayolle, E. C., Öberg, K., Cuppen, H. M., Visser, R., & Linnartz, H. 2011, A&A, 529, A74
Garrod, R. T., Jin, M., Matis, K. A., et al. 2022, ApJS, 259, 1
Gavino, S., Dutrey, A., Wakelam, V., et al. 2021, A&A, 654, A65
Gavino, S., Kobus, J., Dutrey, A., et al. 2023, A&A, 680, A59
Gudipati, M. S., Fleury, B., Wagner, R., et al. 2023, Faraday Discuss., 245, 467
Hama, T., & Watanabe, N. 2013, Chem. Rev., 113, 8783
Hoch, K. K. W., Konopacky, Q. M., Theissen, C. A., et al. 2023, AJ, 166, 85
Johansen, A., Oishi, J. S., Mac Low, M.-M., et al. 2007, Nature, 448, 1022
Khanna, R., & Moore, M. 1999, Spectrochim. Acta A: Mol. Biomol. Spectrosc., 55, 961
Kipfer, K., Ligterink, N., Rubin, M., et al. 2024a, A&A, 686, A102
Kipfer, K. A., Galli, A., Riedo, A., et al. 2024b, Icarus, 410, 115742
Kouchi, A., & Yamamoto, T. 1995, Progr. Cryst. Growth Character. Mater., 30, 83
Krijt, S., Schwarz, K. R., Bergin, E. A., & Ciesla, F. J. 2018, ApJ, 864, 78
Krijt, S., Bosman, A. D., Zhang, K., et al. 2020, ApJ, 899, 134
Lambrechts, M., & Johansen, A. 2012, A&A, 544, A32
Lambrechts, M., Morbidelli, A., Jacobson, S. A., et al. 2019, A&A, 627, A83
Ligterink, N., & Minissale, M. 2023, A&A, 676, A80
Ligterink, N., Walsh, C., Bhuin, R., et al. 2018, A&A, 612, A88
Ligterink, N. F. W., Kipfer, K. A., Rubin, M., et al. 2024, A&A, 687, A78
Line, M. R., Brogi, M., Bean, J. L., et al. 2021, Nature, 598, 580
Linnartz, H., Ioppolo, S., & Fedoseev, G. 2015, Int. Rev. Phys. Chem., 34, 205
Madhusudhan, N., Harrington, J., Stevenson, K. B., et al. 2011, Nature, 469, 64
Madhusudhan, N., Amin, M. A., & Kennedy, G. M. 2014, ApJ, 794, L12
Madhusudhan, N., Bitsch, B., Johansen, A., & Eriksson, L. 2017, MNRAS, 469, 4102
Marks, J. H., Wang, J., Sun, B.-J., et al. 2023, ACS Central Sci., 9, 2241
Martín-Doménech, R., Caro, G., Bueno, J., & Goesmann, F. 2014, A&A, 564
May, R. A., Scott Smith, R., & Kay, B. D. 2013a, J. Chem. Phys., 138, 104501
May, R. A., Scott Smith, R., & Kay, B. D. 2013b, J. Chem. Phys., 138, 104502
McClure, M., Bergin, E., Cleeves, L., et al. 2016, ApJ, 831, 167
Minissale, M., Aikawa, Y., Bergin, E., et al. 2022, ACS Earth Space Chem., 6, 597
Mollière, P., Stolker, T., Lacour, S., et al. 2020, A&A, 640, A131
Mordasini, C., van Boekel, R., Mollière, P., Henning, T., & Benneke, B. 2016, ApJ, 832, 41
Noble, J., Theule, P., Duvernay, F., et al. 2014, PCCP, 16, 23604
Notesco, G., Bar-Nun, A., & Owen, T. 2003, Icarus, 162, 183
Notsu, S., Eistrup, C., Walsh, C., & Nomura, H. 2020, MNRAS, 499, 2229
Öberg, K. I., Boogert, A. A., Pontoppidan, K. M., et al. 2011a, ApJ, 740, 109
Öberg, K. I., Murray-Clay, R., & Bergin, E. A. 2011b, ApJ, 743, L16
Owen, J. E. 2020, MNRAS, 495, 3160
Pontoppidan, K. 2006, A&A, 453, L47
Potapov, A., Semenov, D., Jäger, C., & Henning, T. 2023, ApJ, 954, 167
Qasim, D., McLain, H. L., Aponte, J. C., et al. 2023, ACS Earth Space Chem., 7, 156
Rubin, M., Altwegg, K., Berthelier, J.-J., et al. 2023, MNRAS, 526, 4209
Schneeberger, A., Mousis, O., Aguichine, A., & Lunine, J. I. 2023, A&A, 670, A28
Simon, A., Öberg, K. I., Rajappan, M., & Maksiutenko, P. 2019, ApJ, 883, 21
Simon, A., Rajappan, M., & Öberg, K. I. 2023, ApJ, 955, 5
Sturm, J., McClure, M., Beck, T., et al. 2023, A&A, 679, A138
Taquet, V., Ceccarelli, C., & Kahane, C. 2012, A&A, 538, A42
Van Dishoeck, E. F., Herbst, E., & Neufeld, D. A. 2013, Chem. Rev., 113, 9043
van Scheltinga, J. T., Ligterink, N., Bosman, A., Hogerheijde, M., & Linnartz, H. 2022, A&A, 666, A35
van't Hoff, M. L., Walsh, C., Kama, M., Facchini, S., & van Dishoeck, E. F. 2017, A&A, 599, A101
Visser, R., van Dishoeck, E. F., Doty, S. D., & Dullemond, C. P. 2009, A&A, 495, 881
Viti, S., Collings, M. P., Dever, J. W., McCoustra, M. R., & Williams, D. A. 2004, MNRAS, 354, 1141
Whittet, D. 2010, ApJ, 710, 1009
Zhang, K., Bosman, A. D., & Bergin, E. A. 2020a, ApJ, 891, L16
Zhang, K., Schwarz, K. R., & Bergin, E. A. 2020b, ApJ, 891, L17
Zhang, Y., Snellen, I. A., Bohn, A. J., et al. 2021, Nature, 595, 370

Appendix A: Trapping fractions

Table A.1 shows the trapped fractions of volatiles obtained from various studies. Trapping fractions are usually determined in the following way. In a laboratory setup, an ice film consisting of two or more components is prepared by dosing gas mixture on an ultra-cold (5–80 K) surface. Next, the ice is linearly heated in a process called Temperature Programmed Desorption (TPD) with heating rates that are generally a few K min^{-1}. A mass spectrometer records the molecules desorbing from the ice film at their characteristic mass-over-charge (m/z), for example, m/z=18 for H_2O^+, m/z=28 for CO^+, and m/z=44 for CO_2^+, see Fig. 1. From the TPD trace, desorption and trapping fractions are determined by integrating the signal over a specified temperature regime that corresponds to a certain desorption event. For example, Kipfer et al. (2024a) determines CO desorption fractions by integrating between 15–60 K for pure CO, 60–115 K for CO co-desorption with CO_2, and 115–200 K for CO release associated with water (this combines the so-called volcano desorption event and the water co-desorption into one). Between different studies, integration ranges can differ slightly, but this does not significantly affect determined fractions due to the intensity of desorption events (note the logarithmic scale in Fig. 1).

Various studies provide relevant TPD data, but without determining desorption or trapping fractions. In these cases, fractions can be retrieved by analysing digitised TPD traces, see for example Rubin et al. (2023), where fractional desorption is determined for TPD data from Kouchi & Yamamoto (1995) and Gudipati et al. (2023). For this study, we additionally analyse TPD data from Collings et al. (2004) and Martín-Doménech et al. (2014). Integration range are set from $T_{\rm start}$–60 K for pure CO desorption, 60–130 K for pure CO_2 desorption and CO co-desorption, and 130–200 K for CO and CO_2 release associated with H_2O sublimation, where $T_{\rm start}$ is the lowest temperature presented in the TPD trace.

Some nuances are important to be aware of when interpreting desorption data of ice films consisting of three or more components. The desorption behaviour of binary ice mixtures is fairly easy to understand. Usually, a volatile species (e.g. CO) is embedded in a more abundant and less volatile host medium (e.g. CO_2). In these cases, the release of the volatile occurs at its pure-phase sublimation temperature and when the host medium sublimates (for example, see Simon et al. 2019, for experiments of CO trapping in CO_2). Trends in trapping fractions are easy to assess based on mixing ratios and ice film thicknesses. However, when a third component is added such as H_2O, the trapping behaviour of CO in CO_2 is changed, because CO_2 itself interacts with and is trapped in H_2O (see e.g. Kipfer et al. 2024a). This complicates plotting trends of the CO co-release with CO_2, because the pure-phase CO_2 thickness and mixing ratios are difficult to determine and affected by the additional components in the ice. Therefore, the total ice thickness and mixing ratios are used to plot trends in trapping behaviour in ice mixtures consisting of three or more components, but this is not an accurate representation of the ice composition.

Appendix B: Additional plots

Additional model results where not only volatile trapping in H_2O is included, but also CO trapping in CO_2 are shown in Figs. B.1 and B.2. A reduction in C/O variations is again observed, but the release of a fraction of the CO with CO_2 causes a more pronounced drop in solid-state C/O ratio around the CO_2 snowline.

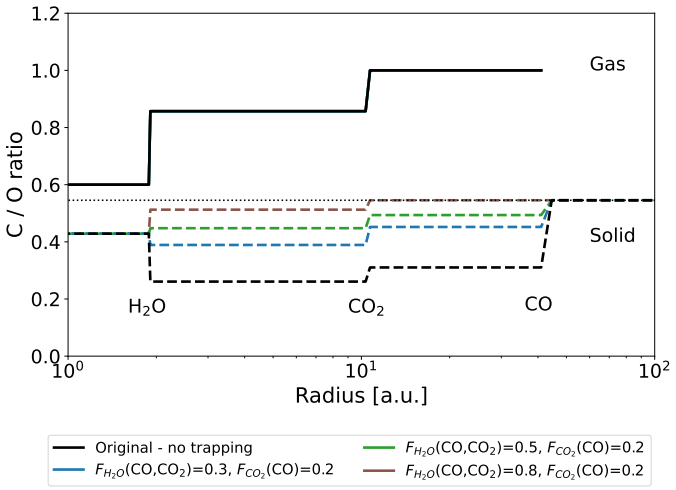

Fig. B.1. Same as Figure 2, but including CO trapping in CO_2. We note that for the model $F_{\rm H_2O}$(CO,CO_2) = 0.8, F_{CO_2}(CO) = 0.2 there is no gas phase C/O ratios outside the CO_2 snowline because CO does not release before the CO_2 co-desorption event.

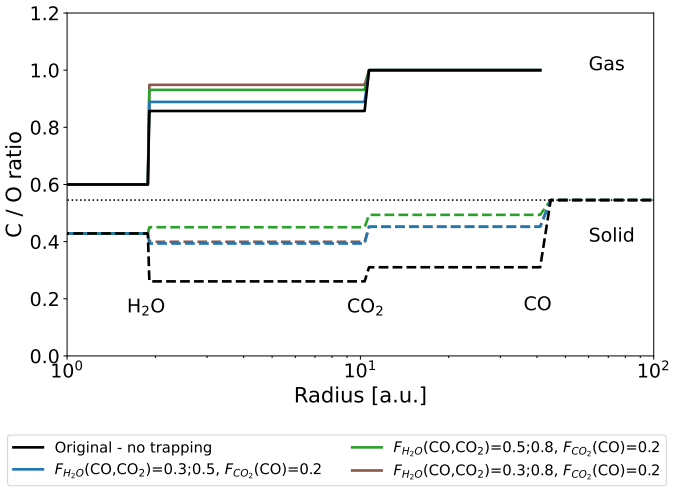

Fig. B.2. Same as Figure 2, but different trapping ratios of CO and CO_2 in H_2O and CO trapping in CO_2.

Table A.1. Volatile trapping experimental results

Molecule	F_{H_2O}(X)	Thickness (ML)	H_2O:X	Reference
CO	[0.41 – 0.64]	1000	[21 – 125]	(Kipfer et al. 2024a)
CO	0.23	1000	6	Gudipati et al. (2023), Rubin et al. (2023)
CO	[0.27 – 0.61]	[14 – 69]	[3 – 10]	Simon et al. (2023)
CO	[0.36 – 0.61]	[309 – 1396]	[6.7–11.5]	Martín-Doménech et al. (2014)[a]
CO	[0.04 – 0.96]	[14 – 30]	[1 – 20]	Fayolle et al. (2011)
CO	0.21	105	20	Collings et al. (2004)[a]
CO	0.07	≥1000	4.3	Kouchi & Yamamoto (1995), Rubin et al. (2023)
CO_2	0.55	1000	3	Gudipati et al. (2023), Rubin et al. (2023)
CO_2	[0.76 – 0.94]	[750 – 1396]	[5 – 10]	Martín-Doménech et al. (2014)[a]
CO_2	[0.32 – 0.92]	[14 – 30]	[3 – 20]	Fayolle et al. (2011)
CO_2	0.34	105	20	Collings et al. (2004)[a]
CO_2	0.20	≥1000	6.5	Kouchi & Yamamoto (1995), Rubin et al. (2023)
Molecule	F_{CO_2}(CO)	Thickness (ML)	CO_2:CO	Reference
CO	[0.11 – 0.34]	1000	[2 – 28]	Kipfer et al. (2024a)
CO	0.07	≥1000	0.67	Gudipati et al. (2023), Rubin et al. (2023)
CO	[0.33 – 0.67]	[13 – 72]	[3 – 13]	Simon et al. (2023)
CO	[0.14 – 0.60]	[6 – 53]	[1 – 9]	Simon et al. (2019)
CO	0.17	1000	2	Kouchi & Yamamoto (1995), Rubin et al. (2023)

Notes. F_{H_2O}(x) indicates the fraction of CO or CO_2 trapped in water. F_{CO_2}(CO) indicates the fraction of CO trapped in CO_2. The thickness is indicated in monolayers (ML), where 1 ML = 10^{15} molecules cm^{-2}. [a]Trapping fractions determined in this work.